A novel physiological role for ARF1 in the formation of bidirectional tubules from the Golgi

Francesca Bottanelli[a], Nicole Kilian[a], Andreas M. Ernst[a], Felix Rivera-Molina[a], Lena K. Schroeder[a], Emil B. Kromann[a,b], Mark D. Lessard[a], Roman S. Erdmann[a,c], Alanna Schepartz[c,d], David Baddeley[a,e], Joerg Bewersdorf[a,b,e], Derek Toomre[a,e], and James E. Rothman[a,e,*]
[a]Department of Cell Biology, Yale University School of Medicine, New Haven, CT 06520; [b]Department of Biomedical Engineering, [c]Department of Chemistry, and [d]Department of Molecular, Cellular, and Developmental Biology, Yale University, New Haven, CT 06520; [e]Nanobiology Institute, Yale University, West Haven, CT 06516

ABSTRACT Capitalizing on CRISPR/Cas9 gene-editing techniques and super-resolution nanoscopy, we explore the role of the small GTPase ARF1 in mediating transport steps at the Golgi. Besides its well-established role in generating COPI vesicles, we find that ARF1 is also involved in the formation of long (~3 μm), thin (~110 nm diameter) tubular carriers. The anterograde and retrograde tubular carriers are both largely free of the classical Golgi coat proteins coatomer (COPI) and clathrin. Instead, they contain ARF1 along their entire length at a density estimated to be in the range of close packing. Experiments using a mutant form of ARF1 affecting GTP hydrolysis suggest that ARF1[GTP] is functionally required for the tubules to form. Dynamic confocal and stimulated emission depletion imaging shows that ARF1-rich tubular compartments fall into two distinct classes containing 1) anterograde cargoes and clathrin clusters or 2) retrograde cargoes and coatomer clusters.

INTRODUCTION

ADP-ribosylation factor (ARF) family proteins are GTPase regulators of vesicle coat assembly and disassembly (Donaldson and Jackson, 2011). Their activation cycle is tightly spatially and temporally regulated by guanine nucleotide exchange factors (GEFs) that catalyze exchange of GDP with GTP on ARFs and GTPase-activating proteins (GAPs), which catalyze the hydrolysis of GTP on ARFs. The most abundant (Popoff et al., 2011) and well-studied member of the ARF family is ARF1, which has a well-established role in the assembly and

budding of COPI vesicles at the Golgi (Kahn and Gilman, 1984; Ostermann et al., 1993; Bremser et al., 1999), namely, ARF1[GDP] is recruited to the Golgi membrane by p24 family proteins (Gommel et al., 2001), where it is activated by the GEF GBF1 (Claude et al., 1999). Active ARF1[GTP] then recruits coatomer (Serafini et al., 1991; Palmer et al., 1993) for the formation of COPI-coated vesicles.

Visualization of the dynamics and nanoscale organization of ARF1 in living cells has been challenging due to the difficulty of imaging molecular processes in the intrinsically crowded perinuclear area using standard, diffraction-limited imaging techniques. Another limitation lies in the overexpression of single components of such machinery, as these processes are tightly regulated at the endogenous level, and any stoichiometric disturbance could result in artifacts.

In addition to its role in COPI vesicle biogenesis implicated in retrograde and intra-Golgi transport, ARF1 has been also shown to control the budding of a wide variety of other types of coated vesicles. It recruits the adaptor protein complexes AP1, AP3, and AP4, as well as GGA complexes (Stamnes and Rothman, 1993; Traub et al., 1993; Ooi et al., 1998; Boehm et al., 2001; Bonifacino, 2004) and exomer complexes (Paczkowski and Fromme, 2014) at the trans-Golgi network (TGN).

Technological advances in the field of live-cell light microscopy imaging in recent years have enabled tubular transport intermediates to be visualized alongside classical transport vesicles (Martinez-Alonso et al., 2013). Both anterograde (ER-to-Golgi) and retrograde

(Golgi-to-ER) markers have been observed in putative tubular transport intermediates (Presley et al., 1997, 1998; Sciaky et al., 1997), suggesting a role for tubular transport at the ER–Golgi interface. The small GTPase Rab6 is believed to be involved in a COPI-independent tubular-vesicular retrograde pathway from the Golgi back to the ER (White et al., 1999; Sengupta et al., 2015). Tubular post-Golgi transport intermediates have also been observed when imaging pulsed anterograde cargo such as Vesicular Stomatitis virus Glycoprotein (VSV G; Hirschberg et al., 1998; Toomre et al., 1999; Polishchuk et al., 2003) and E-cadherin (Lock and Stow, 2005).

There is little insight into the molecular mechanisms that produce tubules from Golgi membranes, probably accounting for the slow rate of progress being made in their detailed characterization. Several molecular mechanisms are known to produce or stabilize tubules from plasma membranes (McMahon and Boucrot, 2011) and from endosomes (Cullen, 2008); however, none of the proteins responsible in these cases has been reported to be located in the Golgi, suggesting that other tubulation mechanisms must be involved there. In this regard, it is important that Beck et al. (2008) discovered that ARF1[GTP], acting as a dimer, can drive artificial lipid membranes into tubules and suggested a structural mechanism that could explain this finding. However, the physiological relevance of this important observation was difficult to establish due to the presence of endogenous ARF1 (Krauss et al., 2008). Another mechanism that has been suggested is that certain membrane lipids might contribute to deforming membranes into tubules based on their local production combined with their intrinsic propensity for curvature. Specifically, two lipid-modifying enzymes, lysophosphatidic acid acyltransferase-γ and phospholipase A2-α, were demonstrated to have the ability to modulate the fission of tubules into COPI vesicles in vitro (Yang et al., 2011).

To investigate more effectively the possible role of ARF1 in Golgi-derived tubule formation, we combined gene editing to visualize tagged ARF1 (and related proteins) at endogenous expression levels with super-resolution imaging. This enabled us to definitively visualize and establish the composition of individual Golgi-derived tubules in vivo.

RESULTS

ARF1[EN]-Halo localizes to Golgi-derived tubular transport intermediates

Although the role of ARF1 in the recruitment of machinery necessary for the assembly of transport vesicles at both the cis and trans faces of the Golgi is well established through biochemistry and genetics studies, the understanding of the spatiotemporal organization of these events in living cells is very limited (Presley et al., 2002). To be able to image ARF1 at physiological expression levels in living cells, we endogenously tagged ARF1 at its C-terminus with a Halo-tag using clustered regularly interspaced short palindromic repeats (CRISPR)/Cas9. We then compared its localization with overexpressed ARF1-Halo (Figure 1, a–c) and validated the successful gene editing via Western blot (Figure 1d). Strikingly, only endogenous tagging of ARF1 allowed the visualization of multiple concurrent tubular structures throughout the cytoplasm of the cells (Figure 1b and Supplemental Video S1), whereas overexpressed ARF1-Halo exhibited a substantial amount of cytoplasmic background and low occurrence of clearly identifiable tubular structures (Figure 1a); we believe the difficulty in identifying them was due to the high cytoplasmic background of soluble overexpressed (and tagged) ARF1 and the competition with endogenous ARF1. Next we quantified the number of ARF1[EN]-positive tubular structures based on their origin as 1) Golgi-derived tubules and 2) total

cytoplasmic tubules (Figure 1c). An average of 82 ± 31 total cytoplasmic tubules/cell were observed in ARF1[EN]-Halo cells, whereas only 15 ± 11 tubules were observed in cells overexpressing ARF1-Halo. The same trend was observed for Golgi-associated tubules, with 6.7 ± 1.7 tubules/cell in the gene-edited cell line versus 0.4 ± 0.5 tubules/cell when ARF1 was overexpressed. Of note, chemical fixation with 4% paraformaldehyde (PFA) significantly disrupted tubule integrity in all cases (Figure 1c).

We then used stimulated emission depletion (STED) microscopy to better discern cis from trans cisternae, which revealed that ARF1[EN]-Halo was distributed throughout the Golgi stack (Supplemental Figure S1). The remaining peripheral structures labeled by ARF1[EN]-Halo were identified as ER–Golgi intermediate compartments (ERGICs) and recycling endosomes (Supplemental Figure S2). Live-cell STED imaging showed that the diameter (full-width at half-maximum [FWHM]) of the Golgi-derived tubules was 110 ± 20 nm (Figure 1, e–g).

Of importance, the edited cells did not show any defect in secretory transport (Supplemental Figure S3a), strongly supporting that endogenously tagging ARF1 at the C-terminus does not interfere with normal cellular function. In addition, ARF1[EN]-Halo cells are morphologically comparable to unedited cells (Supplemental Figure S3, c–f). Fluorescence recovery after photobleaching experiments showed that ARF1[EN]-Halo cycles on and off the Golgi membranes with a half time of 30 ± 3 s (Supplemental Figure S3g). This rate is approximately twofold slower than previously reported (Presley et al., 2002) when ARF1 was overexpressed. Presumably, increasing the concentration of ARF1 in the cytosol by overexpression is expected to increase the rate of association of ARF1[GTP] to the Golgi and could readily explain this difference, which underscores the importance of mammalian gene-editing techniques to address native function. We also confirmed that ARF1[EN]-Halo dissociated from the membrane in the presence of the ARF1 nucleotide exchange inhibitor brefeldin A (BFA; Supplemental Figure S4). We do not believe that the Halo-tag or its structural features induced tubulation, as Golgi-proximal tubules were also observed with enhanced green fluorescent protein (EGFP)-, SNAP-, and hemagglutinin (HA)-tagged (under glutaraldehyde fixation) genome-edited ARF1 (Supplemental Figure S5). Of importance, ARF1[EN]-Halo–positive tubules were also observed in a haploid (HAP1; Essletzbichler et al., 2014) gene-edited cell line (Supplemental Figure S6), ruling out that ARF1[EN]-Halo diffuses into the tubules only as (passive) cargo in the heterozygous HeLa cell line.

ARF1 GTPase activity is required for the formation of Golgi-derived tubules

When ARF1 binds GTP, it changes its conformation to expose its N-terminal myristoylated amphipathic helix, leading to its insertion into Golgi membranes. Indeed, it is this insertion that results in the tubulation of artificial bilayer membranes in vitro (Beck et al., 2008). This was also observed in cells when ARF1 was overexpressed (Krauss et al., 2008). However, the relevance of these observations was unclear because nonphysiological concentrations were used in both cases.

To test whether, at physiological concentrations, ARF1[EN]-Halo GTPase activity is a major factor in tubulation of Golgi membranes, we overexpressed either wild-type ARF1-GFP or the "on"-mutant ARF1-Q71L-GFP (slower GTP hydrolysis rates) in ARF1[EN]-Halo cells and monitored the frequency and length of the tubular ARF1[EN]-Halo–positive transport intermediates in time-lapse experiments (Figure 2). In cells expressing relatively low concentrations of ARF1-Q71L-GFP (corresponding to an average mean GFP intensity at the
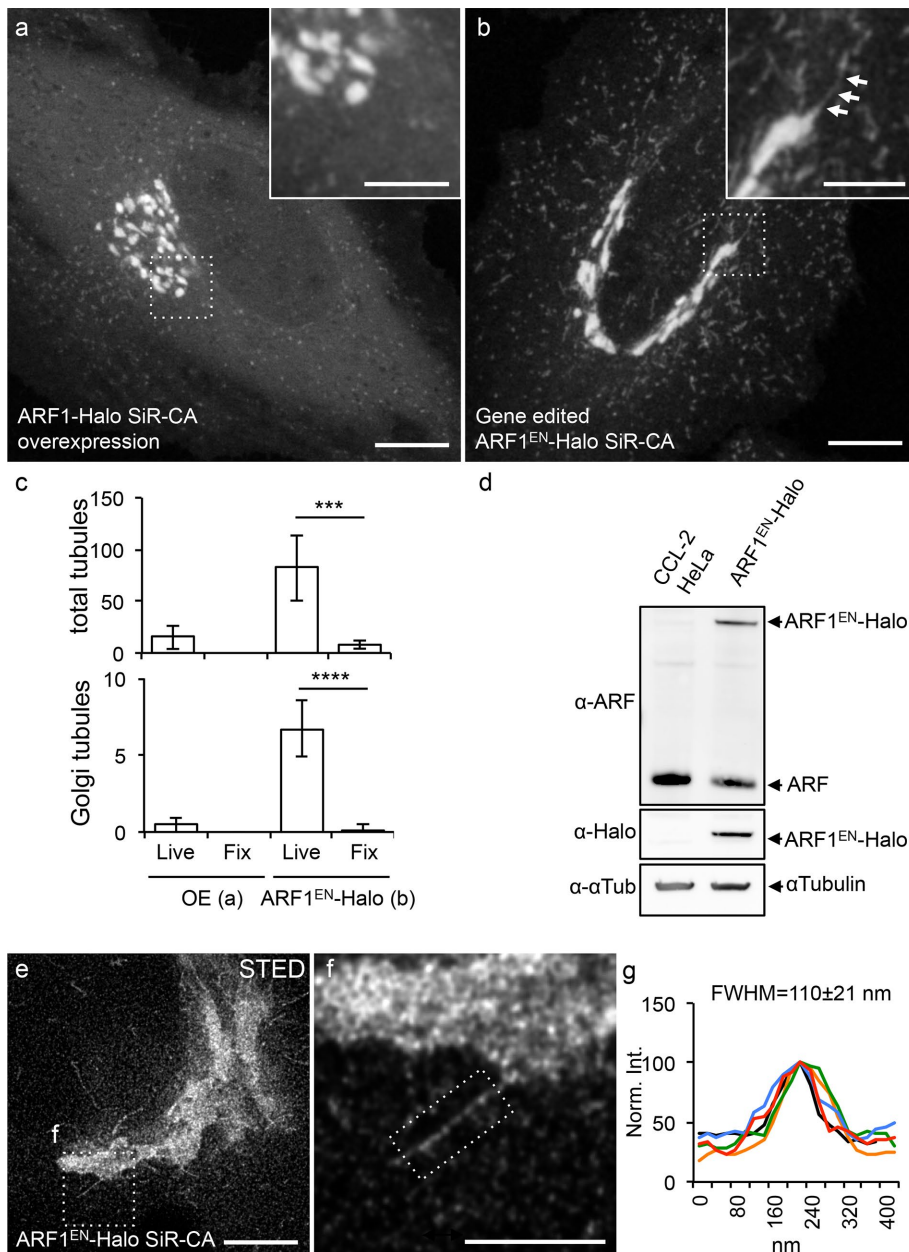
FIGURE 1: Endogenous tagging of ARF1 highlights Golgi-derived tubular structures. Cells either transiently overexpressing ARF1-Halo (a) or expressing gene-edited ARF1^{EN}-Halo (b) were labeled with SiR-CA and imaged with a confocal microscope. (b) A Golgi-derived tubule is highlighted by arrows. (c) Total numbers of tubules/cell and Golgi-derived tubules/cell were quantified in both cells both live and after fixation with 4% PFA. Result of a two-tailed, unpaired *t* test. ***$p < 0.001$, ****$p < 0.0001$ ($n = 10$ cells). (d) Gene editing was validated via Western blot using an antibody that recognizes class I ARFs (ARF1 and ARF3) due to the high protein sequence homology. The added amounts of ARF1^{EN}-Halo (~35%) and unedited ARF (~70%) in the ARF1^{EN}-Halo cell line match the amount of ARF1 (set to 100%) in CCL-2 HeLa cells. (e, f) ARF1^{EN}-Halo cells were imaged on a custom-built STED setup. (g) The average width (FWHM) of the Golgi tubules was 110 ± 21 nm ($n = 20$). All STED images were deconvolved; the line profile represents raw image data. All error bars represent SD. Scale bars, 10 µm (a, b), 5 µm (cropped images, a, b), 5 µm (e), 2 µm (f).

Q71L-GFP, the frequency of Golgi tubules dropped drastically (Figure 2, c and e). The underlying mechanism of this second phenomenon is not known, but GTP hydrolysis might be needed to both initiate the tubules and ultimately limit their growth.

ARF1-regulated anterograde tubular carriers attach to microtubules that guide them toward the cell periphery

To test whether the movement of ARF1^{EN}-Halo-labeled tubular carriers is microtubule dependent, we treated ARF1^{EN}-Halo cells with the microtubule-depolymerizing drug nocodazole (Figure 3, a–d). Using time-lapse experiments, we quantified the length (Figure 3c) and frequency (Figure 3d) of Golgi-derived tubules per minute. Untreated cells exhibited an average tube length of 2.9 ± 1.6 µm with a frequency of 7.8 ± 3.7 tubules/min, whereas nocodazole-treated cells exhibited a significant drop to 1.5 ± 1.2 µm with a frequency of 1.4 ± 1.1 tubules/min, indicating a clear dependence on polymerized microtubules. To image the relationship between microtubules and ARF1 tubules, we took advantage of a recently developed labeling strategy for two-color STED imaging in living cells (Bottanelli et al., 2016) using the STED-compatible dye pair siliconized rhodamine (SiR), in the form of the microtubule probe SiR-tubulin (Lukinavicius et al., 2013, 2014), and ATTO590 to label ARF1^{EN}-Halo. Live-cell STED time lapses highlight that Golgi-derived tubules appeared to extend along and travel on microtubule tracks (Figure 3, e–g), as ARF1 tubules extensively colocalized with microtubules in space and time.

We next tracked the tubules to gain insight into the directionality of transport. Tubules emerging from the Golgi exhibited an average speed of 0.99 ± 0.05 µm/s (Figure 3, h and i), which is comparable to the velocity of motor proteins traveling along microtubules such as kinesin or dynein (Muller et al., 2010). Estimates of the pattern of optical flow around the Golgi were carried out with the Python Microscopy Environment (PYME; http://david_baddeley .bitbucket.org/python-microscopy/; see the Supplemental Methods). ARF1^{EN}-Halo shows a modest bias for outward versus inward flow (Figure 3, j and k), indicative of net movement of ARF1^{EN}-Halo-positive structures away from the Golgi area. One simple interpretation of this would be that some tubules are headed toward the cell periphery, whereas others are headed inward. Note, however, that the ARF1^{EN}-Halo flow measurements do not explicitly segment tubules but also include the motion of ARF1-positive ERGIC and endosomal compartments, as well as the Golgi edge, all of which are observed to "wiggle" in place.

Golgi of 65 ± 24 A.U.), we observed a significant increase in the length of the ARF1^{EN}-Halo tubules (4.5 ± 1.4 µm; Figure 2, b and d) compared with cells expressing similar concentrations of wild-type ARF1-GFP (2.8 ± 0.5 µm; Figure 2, a and d). Of interest, in the population of cells with higher concentrations of Golgi-localized ARF1-
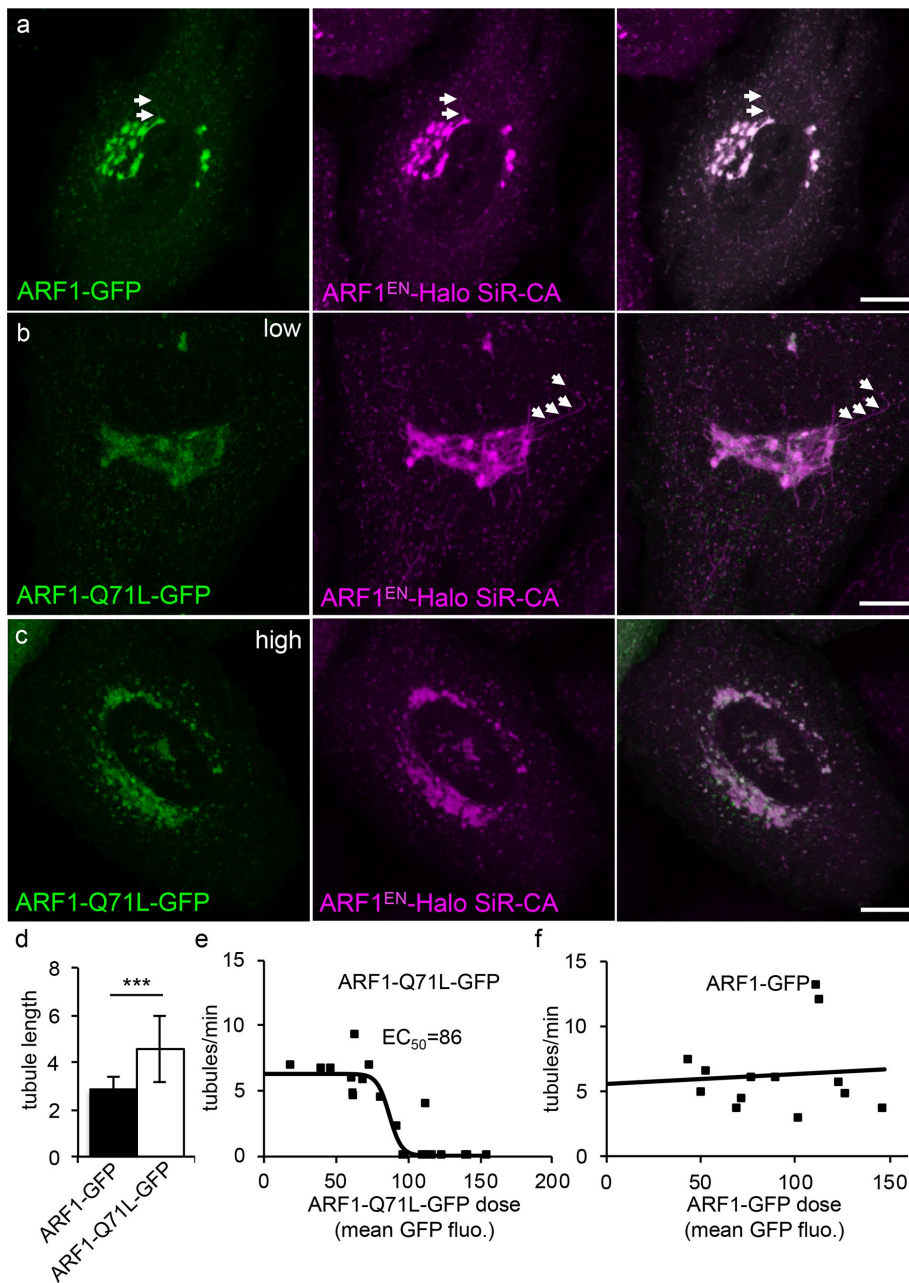
FIGURE 2: ARF1 GTPase activity is required for the formation of Golgi-derived tubules. ARF1[EN]-Halo cells (magenta) were electroporated with plasmids encoding for (a) ARF1-GFP and for ARF1-Q71L-GFP (green) at (b) low and (c) high expression levels. (a, b) Examples of tubules are highlighted by arrows. (d) Cells expressing low levels of ARF1-Q71L-GFP show a significant increase in the length of tubules. Result of a two-tailed, unpaired t test.***$p < 0.001$ (ARF1-GFP, 13 cells; ARF1-Q71L-GFP, 20 cells). (e) When the mean GFP fluorescence at the Golgi of ARF1-Q71L-GFP reaches a certain threshold (86 A.U.), the frequency of tubules drops drastically. Data points from 20 different time-lapse experiments were fitted to a sigmoidal curve (ARF1-Q71L-GFP). (f) No change in frequency of the tubules is observed when ARF1-GFP is overexpressed (13 time-lapse experiments). Error bars represent SD. Scale bars, 10 μm.

ARF1[EN]-Halo tubules also contain clathrin. Because clathrin is tightly packed in the perinuclear area in proximity to the Golgi, STED imaging is necessary to elucidate the spatial relationship between ARF1[EN]-Halo and clathrin (Figure 4). SNAP–clathrin light chain (CLC) clusters were observed on many of the ARF1[EN]-Halo tubules emanating from the Golgi (Figure 4, a–c, and Supplemental Video S2). The clathrin-containing clusters were ~100 nm (99 ± 24 nm) in size (Figure 4d) and appeared as puncta that were distributed in an irregular manner along the length of the tubules, consistent with clathrin-coated buds. There was no enrichment of ARF1[EN]-Halo in the SNAP-CLC buds (Figure 4e). As per the relative frequency of clathrin buds, 73 ± 13% (corresponding to 4.5 ± 1.2 tubules/Golgi) of the ARF1[EN]-Halo tubular structures emanating from the main Golgi body were decorated by SNAP-CLC (Figure 4f).

Multiple distinct carriers form at the TGN and shuttle distinct cargoes to the plasma membrane (Guo *et al.*, 2014). The fact that these tubules contained ARF1[EN]-Halo along their length and also clathrin clusters implied that they may form at the TGN, which is the site of ARF1-dependent clathrin-coated vesicles budding from the Golgi (Stamnes and Rothman, 1993; Traub *et al.*, 1993). If these are indeed anterograde-directed carriers, these tubules should contain at least a subset of anterograde-directed cargoes. Possible candidate cargoes include "nonraft" cargo exemplified by VSV G protein (Keller *et al.*, 2001) and "raft"-directed glycosylphosphatidylinositol (GPI)-anchored proteins (Deng *et al.*, 2016) (Figure 5). To distinguish between these possibilities, we first used an engineered GPI-containing protein that spontaneously aggregates in the ER to prevent its exit. Exit is then triggered by drug-induced depolymerization (Rivera *et al.*, 2000). When released from its aggregated state in the ER, the "raft" cargo GFP-FM4-GPI was rarely observed (only in 3 ± 5% of the cases) in the ARF1[EN]-Halo tubules (Figure 5, a–c and f). GPI-anchored proteins are known to cluster into specialized lipid budding platforms at the TGN that are enriched in sphingolipids, sterols, and saturated lipids (Surma *et al.*, 2012).

To test a "nonraft" class of anterograde cargo, we used a reversible temperature-sensitive folding mutant of VSV G (ts045)

Because these structures comprise a larger fraction of the ARF1[EN]-Halo labeling than the tubular structures, they account for the bulk of the back-and-forth motion, and we expect the net motion of tubular carriers to be significantly higher.

The observed trend for net outward flow of ARF1-positive structures, together with the interaction of ARF1 with clathrin adaptors at the TGN (Guo *et al.*, 2014), prompted us to test whether some of the

that accumulates in the ER at the restrictive temperature but then folds and exits from the ER after shifting to the permissive temperature of 32°C. Thirty minutes after triggering release from the ER, VSV G–SNAP was strikingly observed in 80 ± 13% of ARF1[EN]-Halo–positive, Golgi-derived tubules (Figure 5, d, e, and g, and Supplemental Video S3). This was further supported by two-color STED of VSV G–SNAP and CLC-Halo, which showed that the
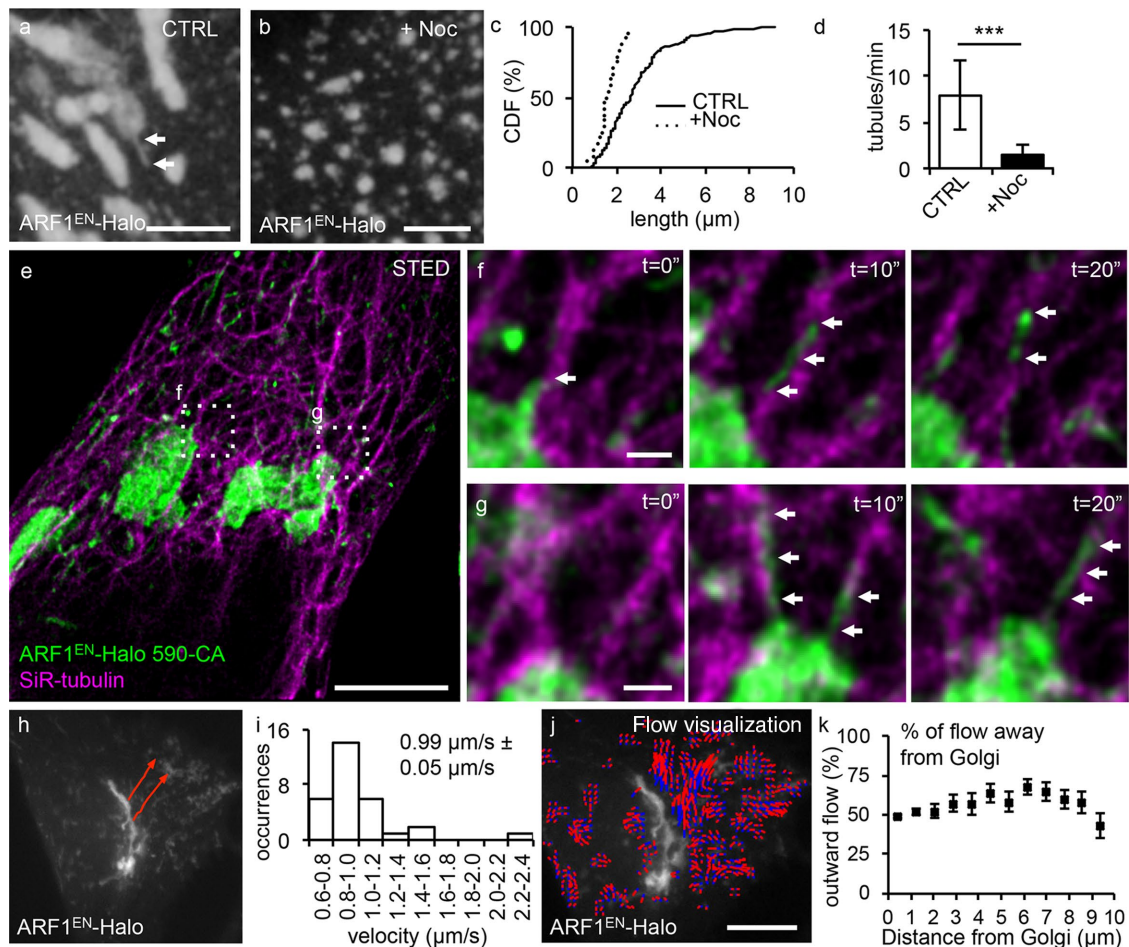
FIGURE 3: ARF1[EN]-Halo tubules move toward the cell periphery on microtubule tracks. The length and frequency of tubules in (a) untreated control (CTRL) ARF1[EN]-Halo cells and (b) nocodazole-treated (+Noc) ARF1[EN]-Halo cells. (c) In nocodazole-treated cells, the length of the tubules is strongly reduced, as shown by the cumulative distribution functions (CDF) of both treated and control cells. (d) In addition, the frequency of the tubules is greatly reduced. Results of a two-tailed, unpaired t test. ***$p < 0.001$ (10 time-lapse movies for both CTRL and +Noc cells). (e–g) ARF1[EN]-Halo (green) cells were treated with SiR-tubulin (magenta) to label microtubules and imaged on a custom-built STED microscope. (f, g) Examples of tubules emanating from the Golgi are highlighted by arrows. (h) Manual tracking with ImageJ of ARF1[EN]-Halo Golgi-derived tubules reveals (i) an average speed of 0.99 ± 0.05 μm/s. (j, k) Quantification of the outward optical flow of ARF1[EN]-Halo fluorescence with respect to the distance from the perinuclear Golgi. (j) ARF1[EN]-Halo flow is represented as blue-to-red arrows to visualize directionality. ARF1[EN]-Halo flow shows a modest bias for outward vs. inward flow. All STED images were deconvolved. Error bars represent SD (d) and SEM (i, k). Scale bars, 5 μm (a, b), 5 μm (e), 500 nm (f, g), 10 μm (h–j).

Golgi-derived, VSV G–positive tubules are also decorated by clathrin clusters (Supplemental Figure S7). Although ARF1[EN]-Halo–positive tubules and VSV G-SNAP colocalize when exiting the Golgi (Figure 5, d and e), these carriers were not observed to fuse with the plasma membrane (Supplemental Figure S8), which suggests that ARF1[EN]-Halo may mainly be involved in the formation of TGN-to-cell periphery carriers and that final delivery of cargo requires a further sorting step.

A subpopulation of ARF1[EN]-Halo-coated tubular intermediates are retrograde Golgi-to-ER carriers

The previous experiments support that ~70% of the Golgi-derived tubules are directed anterograde, carrying cargo such as VSV G protein, and are decorated with clusters of clathrin. One attractive possibility is that the remaining ~30% of the ARF1-containing tubules carry retrograde cargo and may be positive for coatomer (COPI), which is recruited to Golgi membranes by ARF1.

Testing this hypothesis required cells containing tagged coatomer and ARF1 both expressed at endogenous levels. We used CRISPR/Cas9 genome editing to insert the coding sequence for the SNAP tag downstream of the β-COP gene in the ARF1[EN]-Halo background (Figure 6). The β-COP[EN]-SNAP protein localizes to the rims of the Golgi (Figure 6, a and b) and peripheral ARF1[EN]-Halo–positive ERGIC puncta (Figure 6, a and c). Western blot analysis showed that β-COP[EN]-SNAP is the dominant species and the untagged β-COP is hardly expressed (Figure 6d). Of importance, the double-gene-edited cells did not exhibit any functional and morphological defects (Supplemental Figure S3).

Next we used deep–total internal reflection fluorescence (TIRF; Tokunaga et al., 2008) dual-color imaging to characterize the spatial relationship between coatomer and ARF1-tubules in live cells at 3 Hz. Strikingly, we observed that the coatomer was present in distinct clusters along some of the ARF1[EN]-Halo tubules, as observed earlier for clathrin (Figure 6e and Supplemental Video S4). The
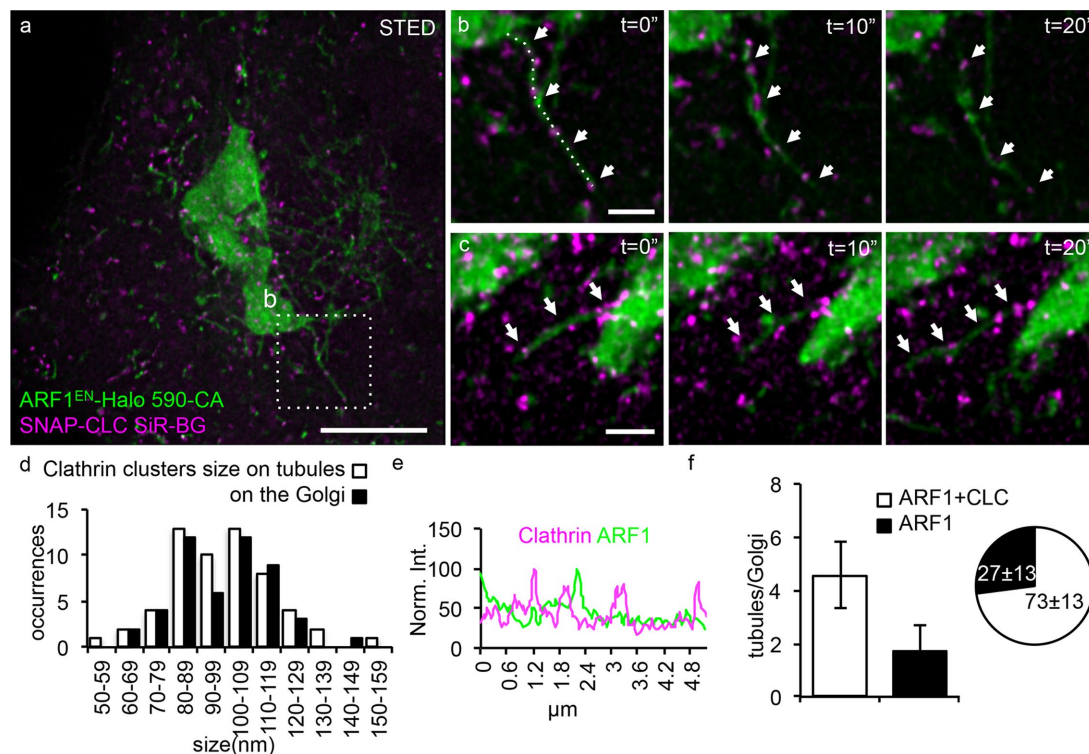
FIGURE 4: The majority of ARF1 tubules are decorated by clathrin clusters. ARF1[EN]-Halo (green) cells were electroporated with a plasmid encoding for SNAP-CLC (magenta). (a–c) Cells were labeled with 590-CA and SiR-BG for two-color live-cell STED imaging on a custom-built microscope. (b, c) Examples of Golgi-derived tubules are highlighted by arrows. (d) A two-dimensional Lorentzian function was fitted to images of clathrin clusters, and FWHM of the fitted functions is represented in histograms. The average size is 99 ± 18 nm for both clathrin clusters on the tubules and on the Golgi (50 clusters). (e) A line profile along the tubule in b shows that there is no enrichment of ARF1 in the clathrin clusters. (f) Quantification of the number of clathrin-positive tubules shows that $73 \pm 13\%$ of the tubules are decorated by SNAP-CLC clusters. All STED images were deconvolved; the line profile represents raw image data. Error bars represent SD. Scale bars, 5 µm (a), 1 µm (b, c).

separations between the coatomer clusters along the length of these tubules remain constant until the tubules collapse into a point-shaped object, likely reflecting fusion with the target membrane (Figure 6e).

These studies were further extended using live-cell STED imaging experiments in which β-COP[EN]-SNAP and ARF1[EN]-Halo were labeled with SiR-BG and 590-CA, respectively (Figure 6, f–k), allowing us to clearly visualize individual ARF1[EN]-Halo–positive tubules extending from the Golgi ribbon. As observed earlier (Figure 4), the staining of β-COP[EN]-SNAP was concentrated in immobile clusters (Figure 6, f and g, and Supplemental Video S5), which was revealed by superresolution to be ~89 ± 24 nm in size, consistent with COPI buds. Of importance, $31 \pm 19\%$ of the observed ARF1[EN]-Halo–positive tubular carriers (corresponding to 2.5 ± 2.3 tubules/Golgi) were also positive for β-COP[EN]-SNAP (Figure 6h), suggesting that the coatomer-decorated tubules account for most of the clathrin-free ARF1-tubules and consistent with the idea that they may be retrograde carriers.

Next we tested whether retrograde markers were enriched in the coatomer-positive ARF1-tubules, using a tagged KDEL-receptor SNAP-tag fusion (KDEL-R-SNAP). This receptor is known to transport KDEL-tagged protein retrograde from the Golgi back to the ER and has been observed in tubular structures (Sciaky *et al.*, 1997; Presley *et al.*, 1998). About $22 \pm 4\%$ of the ARF1[EN]-Halo–positive tubules were found to contain KDEL-R-SNAP (Figure 7, a and c, and Supplemental Video S6). In addition, close to all ($94 \pm 9\%$) of the KDEL-R-GFP–positive tubular structures were found to be decorated

by coatomer clusters when KDEL-R-GFP was expressed in β-COP[EN]-SNAP cells (Figure 7, b and d).

In summary, these data show that there are at least two distinct types of ARF1-dependent/ARF1-containing tubules forming at the Golgi. About two-thirds of the tubules contain anterograde cargo and are sparsely decorated by clathrin clusters along their length. The remaining one-third instead contain retrograde-directed cargo and are sparsely decorated by coatomer clusters along their lengths. ARF1 did not seem to be concentrated in the coatomer clusters on the tubules (Figure 6, i and j). This was particularly surprising because ARF1 was previously found to be highly concentrated in COPI buds compared with surrounding Golgi (Orci *et al.*, 1997). One possibility, considered in the *Discussion*, is that the tubule membrane, unlike the Golgi membrane, is highly enriched in ARF1 due to the mechanism of ARF1-dependent budding.

DISCUSSION

ARF1-dependent bidirectional tubular transport from the Golgi

Endogenously expressed ARF1[EN]-Halo labels transient tubular carriers that are readily observed to form at the Golgi ribbon (Figure 1). The effects of a mutant ARF1 that poorly hydrolyzes GTP (Figure 2) suggest that ARF1[GTP] functions in the formation and/or stability of these tubules. Although modifications at the C-terminus of ARF1 have been suggested to alter ARF1 in vitro kinetics (Jian *et al.*, 2010), we believe that it is unlikely that the Halo-tag or its structural
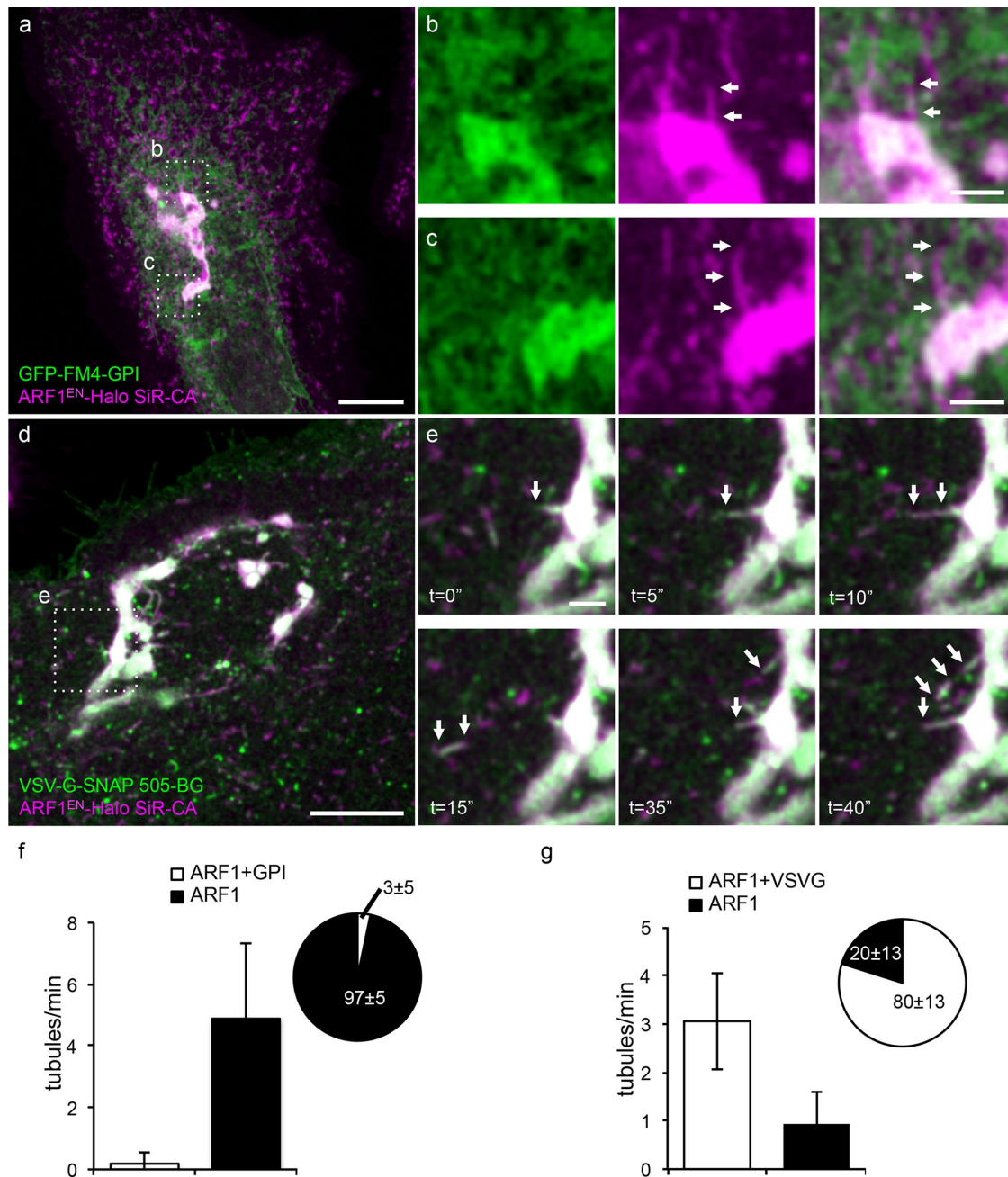
FIGURE 5: ARF1[EN]-Halo post-Golgi tubules contain the anterograde cargo VSV G-SNAP but not the raft-associated cargo GPI-GFP-FM4. ARF1[EN]-Halo cells were electroporated with GFP-FM4-GPI (a–c) and VSV G-SNAP (d, e) encoding plasmids. Cells were labeled with SiR-CA only (a–c) or 505-BG and SiR-CA (d, e). (a) Aggregated GFP-FM4-GPI was released from the ER by adding the disaggregating drug. (a–c) GFP-FM4-GPI was never observed in ARF1[EN]-Halo-positive structures. (b, c) ARF1[EN]-Halo tubules devoid of GFP-FM4-GPI are highlighted by arrows. (d) VSV G-SNAP cells were grown overnight at 40.5°C and then shifted to 32°C on the microscope stage to release the cargo from the ER. (e) At ~30 min after shifting the cells to the permissive temperature, tubules containing both ARF1[EN]-Halo and VSV G-SNAP were observed forming at the Golgi (arrows). (f) A negligible fraction of ARF1[EN]-Halo tubules contained the cargo GFP-FM4-GPI. The frequency of VSV G–positive tubules exiting the Golgi is 3 ± 1 tubules/min, and 80 ± 13% of the ARF1[EN]-Halo tubules also contained VSV G–SNAP (g). Error bars represent SD. Scale bars, 10 μm (a, c), 2 μm (b, d, e).

features induced tubulation, for the following reasons: 1) ARF1-positive, Golgi-proximal tubules were also observed with genome-edited ARF1 tagged with EGFP or SNAP and, under glutaraldehyde fixation, with HA-tagged ARF1 (ARF1[EN]-HA; Supplemental Figure S5); 2) ARF1[EN]-Halo–positive tubules are observed in a gene-edited haploid HAP1 cell line, ruling out that ARF1-Halo did not actively contribute to the tubules observed in the heterozygous HeLa cell line (Supplemental Figure S6); 3) a fraction of ARF1-Halo–positive tubules contain KDEL receptor (Figure 7), and KDEL-positive tubules also are observed in cells with unedited ARF1; 4) no perturbation of cell morphology, and of importance, secretory trafficking was observed in ARF1-HALO edited cell lines; and 5) untagged ARF1 is able to tubulate membranes in vitro (Beck *et al.*, 2008).
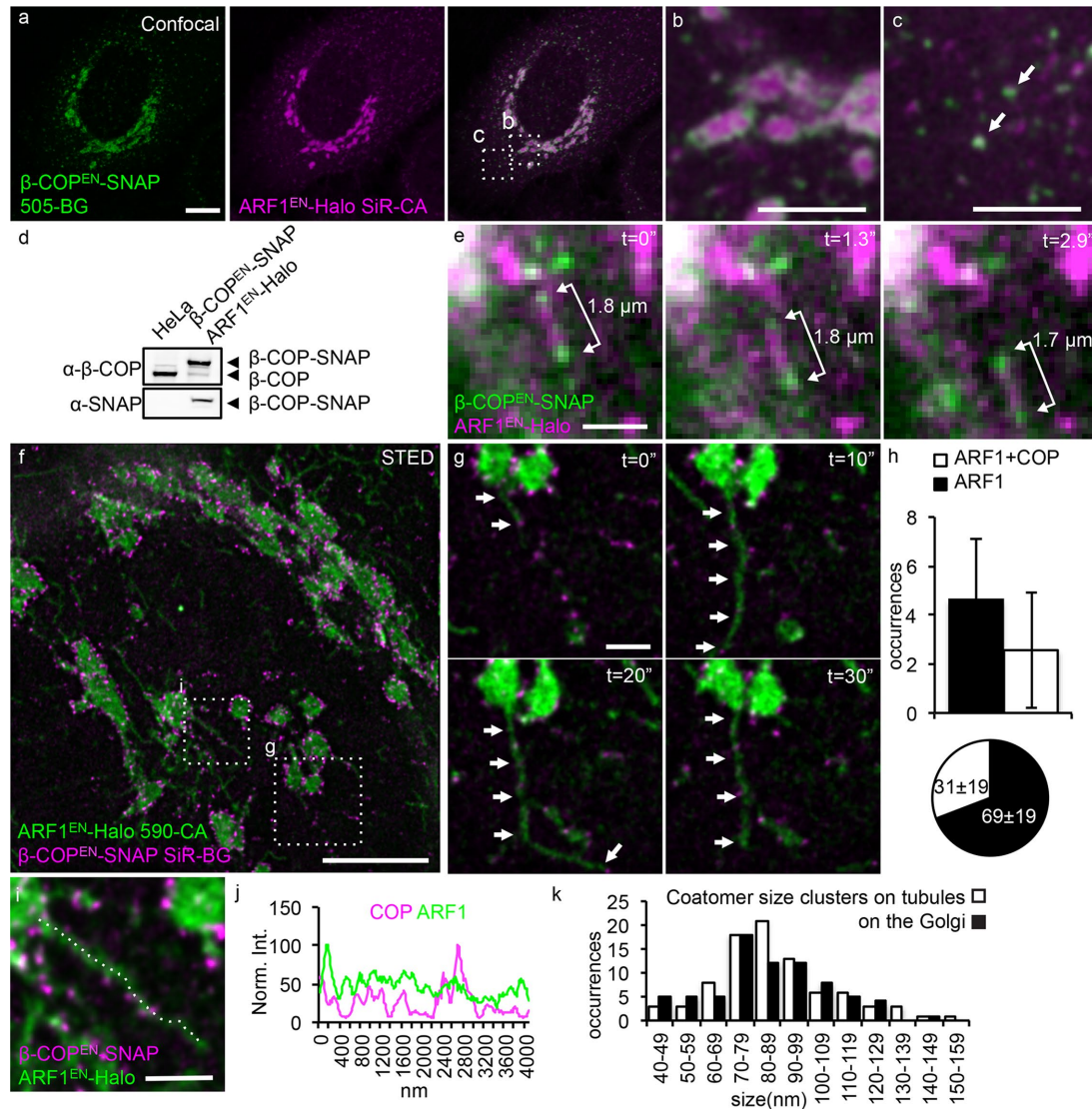
FIGURE 6: Coatomer clusters decorate the remaining fraction of ARF1[EN]-Halo tubules. (a–c) ARF1[EN]-Halo and β-COP[EN]-SNAP double-gene-edited cells were labeled with 505-BG (green) and SiR-CA (magenta) for confocal imaging. β-COP[EN]-SNAP localizes to (b) the rims of the Golgi cisternae and (c) peripheral ERGIC structures. (d) The correct tagging of endogenous β-COP was validated via Western blot. (e) ARF1[EN]-Halo and β-COP[EN]-SNAP cells were imaged with deep-TIRF at a frame rate of ~3 frames/s on an OMX microscope. (e) Golgi-derived tubular structures labeled by ARF1[EN]-Halo and decorated by clusters of β-COP[EN]-SNAP were observed, and the distance between the clusters of coatomer remained constant. (f, g) The same double-gene-edited cells were labeled with 590-CA (green) and SiR-BG (magenta) for live-cell STED imaging on a custom instrument. (h) Single STED frames were used to quantify the number of coatomer-positive tubules/Golgi; 2.5 ± 2.3 tubules/Golgi were decorated by coatomer, which corresponds to 31 ± 19% of the total tubules. (i, j) Line profile along a coatomer-positive tubule shows that there is no enrichment of ARF1[EN]-Halo in the β-COP[EN]-SNAP–positive clusters. (k) A two-dimensional Lorentzian function was fitted to images of coatomer clusters, and FWHM of the fitted functions is represented in histograms. The average size of coatomer clusters on the tubules is 89 ± 24 nm, similar to the size of clusters/buds at the Golgi (86 ± 24 nm). All STED images were deconvolved; the line profile represents raw image data. Error bars represent SD. Scale bars, 10 μm (a), 5 μm (b, c), 2 μm (e), 5 μm (f), 1 μm (g, i).

Beck *et al.* (2008) found that dimers of ARF1[GTP] shape membranes into tubules in vitro according to a simple physical-chemical mechanism in which a pair of spatially separated, solvent-exposed and myristoylated amphipathic helices insert into the outer leaflet, increasing its surface area relative to the inner leaflet. This expansion can only be accommodated by conversion of the ARF1[GTP]-containing region into a tubular geometry. This mechanism necessarily requires that ARF1 occupies a large fraction of the tubule surface and will necessarily concentrate ARF1[GTP] within such tubular regions. If this same mechanism applied in vivo, we would expect that ARF1 would be similarly close packed on the surface of the tubules. We would further expect that such close packing would exclude COPI or clathrin buds that can be triggered by ARF1 binding, because these would require a different local arrangement of ARF1 subunits on the membrane directed by the geometry of coat binding as distinct from that of curved tubule membrane binding.
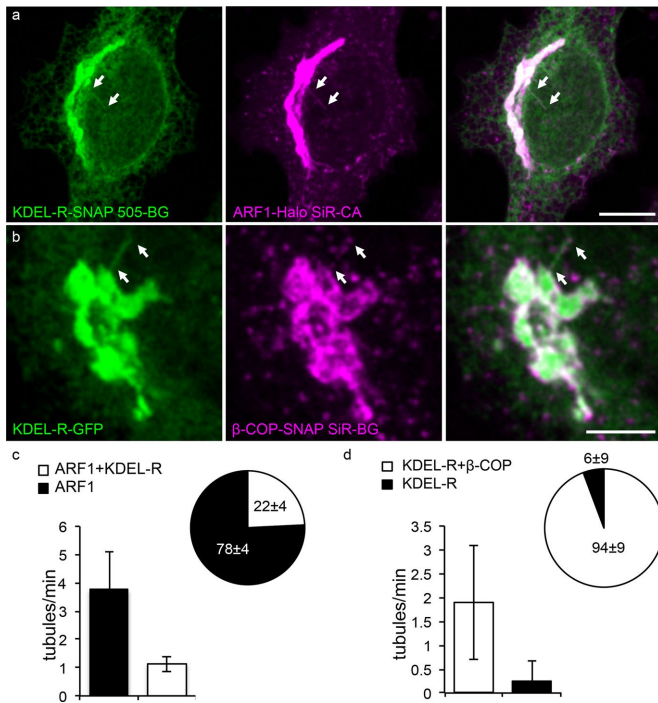
FIGURE 7: Coatomer-positive tubules contain the retrograde marker KDEL receptor. (a) ARF1[EN]-Halo cells were electroporated with a KDEL-R-SNAP–encoding plasmid and labeled with 505-BG and SiR-CA for confocal imaging. KDEL-R-SNAP–containing tubules were also decorated by ARF1[EN]-Halo (arrows). (c) We found that 1.3 ± 0.3 ARF1[EN]-Halo tubules/min also contained KDEL-R, which corresponds to $22 \pm 4\%$ of the total ARF1[EN]-Halo tubules observed. (b) β-COP[EN]-SNAP cells were electroporated with a KDEL-R-GFP–encoding plasmid and labeled with SiR-CA for confocal imaging. Nearly all observed KDEL-R-GFP tubules were positive for Coatomer (arrows). (d) We counted 1.9 ± 1.1 KDEL-R-GFP/ β-COP[EN]-SNAP tubules/min, which corresponds to $94 \pm 9\%$ of the total number of tubules observed. Error bars represent SD. Scale bars, 10 μm (a), 5 μm (b).
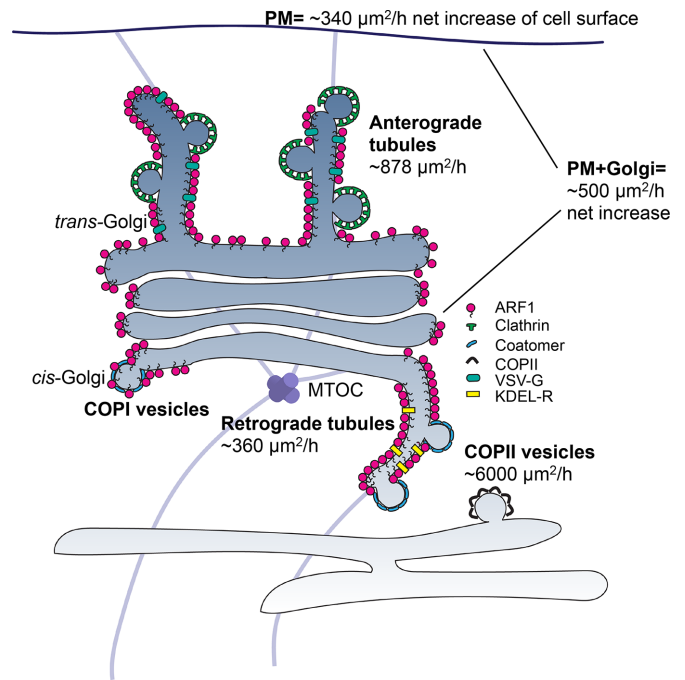
FIGURE 8: ARF1 tubules represent a major membrane flow out of the Golgi. ARF1-dependent retrograde and anterograde tubules are tightly packed with ARF1[EN]-Halo and contain the cargoes KDEL receptor and VSV G, respectively. Clusters of coat proteins (clathrin and coatomer) are observed on the tubules. Retrograde tubules account for a flow of membranes of ~360 μm²/h, ~7% of the flow necessary for membrane balance, if one takes into account the anterograde flow of COPII vesicles (~6000 μm²/h) and the growth of Golgi and post-Golgi membranes (~500 μm²/h). Anterograde tubules account for ~900 μm²/h, approximately threefold of what is needed for plasma membrane (PM) growth (~340 μm²/h). MTOC, microtubule-organizing center.

To test these predictions, we would need to measure the surface concentration (density) of ARF1 on the tubules. Quantitative analysis of our data using independent internal standards (COPI vesicles and microtubules) enabled us to estimate these densities (Supplemental Table S1 and Supplemental Information Note 1). ARF1 is present on both classes of Golgi-derived tubules at ~10,000–20,000 molecules/μm². This is comparable to the density of ARF1 in COPI vesicles (calculated from the cryo–electron microscopy [EM] data of Dodonova *et al.* (2015)) of ~20,000 molecules/μm², and although only an estimate, it suggests that ARF1 literally coats the surface of the tubules, as the simple physical-chemical budding mechanism would suggest. Further in this direction, Dodonova *et al.* (2015) predict that at this density of ARF1 (50–100 nm² per ARF1 molecule), an induced radius of ~100 nm is expected. Because similar ARF1 densities were estimated for the tubules, we conclude that ARF1 is a major driving force for tubulation processes at the Golgi, although other factors, such as the four-phosphate-adaptor protein/specific lipid environment and/or the coats COPI and clathrin, might further contribute to the molecular mechanism of tubule budding (Godi *et al.*, 2004; Deborde *et al.*, 2008).

Our data also suggest that ARF1[EN]-Halo tubules bud en bloc from the Golgi, as previously suggested by Polishchuk *et al.* (2003), and are not formed by homotypic fusion of many small vesicles.

ARF1 tubular transport intermediates can account for a major portion of membrane flow out of the Golgi

The ability to perform time-lapse imaging experiments in living cells expressing tagged ARF1 at its physiological concentration also allows us to roughly estimate the contribution of the ARF1-dependent tubules to the overall flow of membranes in the secretory pathway (Figure 8 and Supplemental Information Note 2). By quantifying the rate of tubule production (number/cell/hour) and their average surface area, we can estimate the total amount of membrane flow and compare it with corresponding estimates of flow via COPII vesicles (ER-to-Golgi) and total membrane synthesis (mass doubling in the cell cycle). A detailed description of the calculations is given in Supplemental Information Note 2.

The rate of flow of membrane out of the ER due to COPII vesicles is estimated to be ~6000 μm²/cell/h (Thor *et al.*, 2009; Barlowe and Helenius, 2016). The net growth of post-ER membrane surface that occurs with each cell doubling consists mainly of Golgi and plasma membrane and for BHK cells is ~3400 μm² for the plasma membrane and ~1700 μm² for the Golgi (Griffiths *et al.*, 1984), totaling ~5100 μm²/cell. This requires ~500 μm²/h of net membrane synthesis over the ~10-h doubling time of a BHK cell. To maintain its surface area in the steady state against the loss due to anterograde flow, the ER in such a cell would therefore need to receive about ~5500 μm²/h (6000 – 500 μm²/h) of surface area returned to it from the Golgi.

Based on these considerations, retrograde ARF1-tubules could account for only ~7% of the area returned to ER to maintain membrane balance. Whereas COPI selects its cargo by binding to the coat, we suggest that ARF tubules may select their cargo based on their intrinsic preference for curvature. If so, retrograde tubules are likely to function in the recycling of specific classes of lipid or protein cargo that are not carried by COPI vesicles. These putative cargoes remain to be identified. Although some KDEL receptors are found in the tubules, the bulk of the recycled KDEL receptors are likely to be carried by COPI, as quantitative immuno-EM studies convincingly documented the concentration of KDEL receptors in Golgi-derived COPI vesicles (Orci et al., 1997). Similarly, it is unlikely that KKXX (and similarly)-tagged ER residents are primarily returned to ER via ARF1 tubules, because these proteins are concentrated in COPI vesicles by directly binding coatomer, and coatomer genes are clearly required for their retrograde transport (Cosson and Letourneur, 1994; Letourneur et al., 1994).

On the other hand, anterograde tubules could account for a very significant portion of anterograde flow of membranes out of the Golgi. The Golgi in each cell produces ~900 μm^2/h of anterograde ARF1-tubes as compared with the ~340 μm^2/cell net increase of cell surface that must be produced in the same period of time. It is not surprising that the estimate of the rate of production of anterograde ARF1 tubules at the Golgi exceeds the net rate of growth of cell surface. These tubules may contribute to intracellular compartments such as endosomes and much of the surface fluxing into the plasma membrane fluxes back inside via a coupled exo-endocytic mechanism. Anterograde ARF1 tubules may represent a quantitatively important exit route from the TGN, although the rate of internalization and recycling from the plasma membrane back to the Golgi has not been taken into account in this study. Tubular carriers have been observed to transport various cargoes toward different post-Golgi destinations, including influenza virus HA– and GPI-anchored proteins to the apical plasma membrane (Keller et al., 2001; Puertollano et al., 2001), VSV G and E-cadherin to the basolateral plasma membrane (Hirschberg et al., 1998; Polishchuk et al., 2003; Lock and Stow, 2005) and mannose-6-phosphate receptor to the endolysosomal system (Puertollano et al., 2003; Waguri et al., 2003). ARF1-positive anterograde carriers contain VSV G but not GPI-linked protein cargo, suggesting a major role of the ARF GTPase in nonraft pathways (Keller et al., 2001), which likely reflects basolateral trafficking in polarized cells.

In summary, we provided physiological evidence for the relevance of a physicochemical tubulation process (Beck et al., 2008) at the Golgi driven by ARF1[GTP] assembly on membranes at both faces of the Golgi stack. It is likely that such post-Golgi tubules are important contributors to the secretory pathway and could potentially carry the majority of certain classes of plasma membrane cargo (represented by VSV G protein). The fusion targets of these tubules remain to be established. ARF1[GTP] is present at similar concentrations throughout the Golgi stack along its *cis–trans* axis (Supplemental Figure S1), and this raises the possibility that analogous tubules may form at the rims of central cisternae in the stack and could represent intercisternal transport intermediates, especially under conditions in which there may be a shortage of available coatomer to pinch them off into vesicles (Trucco et al., 2004; Beznoussenko et al., 2014).

MATERIALS AND METHODS
Cell culture
All experiments were carried out in HeLa cells CCL-2 (American Type Culture Collection) and HAP1 cells (Essletzbichler et al., 2014) grown in an incubator at 37°C with 5% CO_2 in DMEM (Life Tech-

nologies) supplemented with 10% fetal bovine serum (Life Technologies) and penicillin/streptomycin to prevent contamination. Transient transfection of plasmid DNA was carried out using a NEPA21 electroporation system (1×10^6 cells were mixed with 1–10 µg of plasmid DNA, depending on the desired expression levels). Nocodazole, H89, and BFA were all purchased from Sigma-Aldrich and used at the following concentrations: nocodazole, 100 µg/ml; H89, 50 µM; and BFA, 100 µg/ml.

Release of GPI-FM4-GFP was carried out by adding the disaggregating drug D/D solubilizer (Clontech) at a concentration of 1 µM.

For the horseradish peroxidase (HRP) secretion assay, HRP activity in cells and medium samples was assayed using the TMB+ substrate (Dako) following manufacturer's instructions.

Preparation of cells for live imaging
For all of the imaging experiments, cells were seeded on a glass-bottom dish (3.5-cm diameter, No. 1.5; MatTek,) coated with fibronectin (Millipore). For live-cell STED experiments, the dishes were cleaned with 1 M KOH for 15 min in a sonic cleaner before coating. Labeling of living cells with SNAP and Halo substrates for imaging was carried out for 1 h using 1–5 µM stocks. SiR-BG (SNAP-Cell-647) is available from NEB. SiR-CA was a kind gift of Promega. 590-CA was synthesized in the lab as described in Bottanelli et al. (2016). Labeling with SiR-tubulin (Spirochrome) was carried out for 1 h with 1 µM probe. Uptake of Transferrin-568 (ThermoFisher Scientific) was carried out for 1 h at 37°C with 25 µg/ml fluorescent transferrin. An acid wash at pH 5 (50 mM 2-(N-morpholino)ethanesulfonic acid and 150 mM NaCl) was carried out before imaging to remove any transferrin bound to the plasma membrane. All live-cell experiments were carried out at 37°C.

Molecular biology and CRISPR/Cas9 gene editing
See the Supplemental Information

Immunofluorescence
Immunofluorescence was carried out as described previously (Lavieu et al., 2014). Anti-Gpp130 and anti-Golgin97 antibodies were purchased from Covance and Abcam, respectively. Anti-rabbit Atto594 (Rockland), anti-mouse Atto594 (Sigma-Aldrich), and anti-mouse- and anti-rabbit 635P (Abberior) secondary antibodies were used for the STED experiments.

STED imaging
STED imaging was carried out on a recently described custom-built setup (Bottanelli et al., 2016) and on a commercial Leica TCS SP8 STED 3X. Imaging parameters on the custom setup were chosen as described previously (Bottanelli et al., 2016). On the Leica system, 594 and 650 nm were selected as excitation wavelengths on a white-light excitation source for excitation of Atto590/Atto594 or SiR/STAR635P, respectively. HyD 1 and HyD 2 were set to 604- to 644- and 665- to 705-nm detection windows. The 775-nm depletion laser was used to deplete both dyes. The two color channels were imaged sequentially line by line.

Image processing and statistical analysis
For presentation purposes, raw STED images and confocal time lapses were smoothed using a Gaussian filter with 1-pixel SD using ImageJ (Abramoff et al., 2004).

Live-cell STED movies were deconvolved to reduce noise using Richardson–Lucy deconvolution (Richardson, 1972; Lucy, 1974) implemented in the PYME package. Manual tracking was carried out using the manual tracking plug-in of Fiji (Schindelin et al., 2012).

Fittings for Figures 1, 4, and 6 were carried out with Matlab. The curve fitting for Figure 2 and all of the *t* tests were carried out with Prism. Quantification of the optic flow is described in detail in the Supplemental Methods.

REFERENCES

Abramoff MD, Magalhaes PJ, Ram SJ (2004). Image processing with ImageJ. Biophotonics Int 11, 36–42.

Barlowe C, Helenius A (2016). Cargo capture and bulk flow in the early secretory pathway. Annu Rev Cell Dev Biol 32, 197–222.

Beck R, Sun Z, Adolf F, Rutz C, Bassler J, Wild K, Sinning I, Hurt E, Brugger B, Bethune J, et al. (2008). Membrane curvature induced by Arf1-GTP is essential for vesicle formation. Proc Natl Acad Sci USA 105, 11731–11736.

Beznoussenko GV, Parashuraman S, Rizzo R, Polishchuk R, Martella O, Di Giandomenico D, Fusella A, Spaar A, Sallese M, Capestrano MG, et al. (2014). Transport of soluble proteins through the Golgi occurs by diffusion via continuities across cisternae. Elife 3, e02009.

Boehm M, Aguilar RC, Bonifacino JS (2001). Functional and physical interactions of the adaptor protein complex AP-4 with ADP-ribosylation factors (ARFs). EMBO J 20, 6265–6276.

Bonifacino JS (2004). The GGA proteins: adaptors on the move. Nat Rev Mol Cell Biol 5, 23–32.

Bottanelli F, Kromann EB, Allgeyer ES, Erdmann RS, Wood Baguley S, Sirinakis G, Schepartz A, Baddeley D, Toomre DK, Rothman JE, et al. (2016). Two-colour live-cell nanoscale imaging of intracellular targets. Nat Commun 7, 10778.

Bremser M, Nickel W, Schweikert M, Ravazzola M, Amherdt M, Hughes CA, Sollner TH, Rothman JE, Wieland FT (1999). Coupling of coat assembly and vesicle budding to packaging of putative cargo receptors. Cell 96, 495–506.

Claude A, Zhao BP, Kuziemsky CE, Dahan S, Berger SJ, Yan JP, Armold AD, Sullivan EM, Melancon P (1999). GBF1: a novel Golgi-associated BFA-resistant guanine nucleotide exchange factor that displays specificity for ADP-ribosylation factor 5. J Cell Biol 146, 71–84.

Cosson P, Letourneur F (1994). Coatomer interaction with di-lysine endoplasmic reticulum retention motifs. Science 263, 1629–1631.

Cullen PJ (2008). Endosomal sorting and signalling: an emerging role for sorting nexins. Nat Rev Mol Cell Biol 9, 574–582.

Deborde S, Perret E, Gravotta D, Deora A, Salvarezza S, Schreiner R, Rodriguez-Boulan E (2008). Clathrin is a key regulator of basolateral polarity. Nature 452, 719–723.

Deng Y, Rivera-Molina FE, Toomre DK, Burd CG (2016). Sphingomyelin is sorted at the trans Golgi network into a distinct class of secretory vesicle. Proc Natl Acad Sci USA 113, 6677–6682.

Dodonova SO, Diestelkoetter-Bachert P, von Appen A, Hagen WJ, Beck R, Beck M, Wieland F, Briggs JA (2015). VESICULAR TRANSPORT. A structure of the COPI coat and the role of coat proteins in membrane vesicle assembly. Science 349, 195–198.

Donaldson JG, Jackson CL (2011). ARF family G proteins and their regulators: roles in membrane transport, development and disease. Nat Rev Mol Cell Biol 12, 362–375.

Essletzbichler P, Konopka T, Santoro F, Chen D, Gapp BV, Kralovics R, Brummelkamp TR, Nijman SMB, Burckstummer T (2014). Megabase-scale deletion using CRISPR/Cas9 to generate a fully haploid human cell line. Genome Res 24, 2059–2065.

Godi A, Di Campli A, Konstantakopoulos A, Tullio G, Alessi DR, Kular GS, Daniele T, Marra P, Lucocq JM, De Matteis MA (2004). FAPPs control Golgi-to-cell-surface membrane traffic by binding to ARF and PtdIns(4)P. Nat Cell Biol 6, 393–404.

Gommel DU, Memon AR, Heiss A, Lottspeich F, Pfannstiel J, Lechner J, Reinhard C, Helms JB, Nickel W, Wieland FT (2001). Recruitment to Golgi membranes of ADP-ribosylation factor 1 is mediated by the cytoplasmic domain of p23. EMBO J 20, 6751–6760.

Griffiths G, Warren G, Quinn P, Mathieu-Costello O, Hoppeler H (1984). Density of newly synthesized plasma membrane proteins in intracellular membranes. I. Stereological studies. J Cell Biol 98, 2133–2141.

Guo YS, Sirkis DW, Schekman R (2014). Protein Sorting at the trans-Golgi Network. Annu Rev Cell Dev Biol 30, 169–206.

Hirschberg K, Miller CM, Ellenberg J, Presley JF, Siggia ED, Phair RD, Lippincott-Schwartz J (1998). Kinetic analysis of secretory protein traffic and characterization of golgi to plasma membrane transport intermediates in living cells. J Cell Biol 143, 1485–1503.

Jian XY, Cavenagh M, Gruschus JM, Randazzo PA, Kahn RA (2010). Modifications to the C-Terminus of Arf1 alter cell functions and protein interactions. Traffic 11, 732–742.

Kahn RA, Gilman AG (1984). Purification of a protein cofactor required for ADP-ribosylation of the stimulatory regulatory component of adenylate cyclase by cholera toxin. J Biol Chem 259, 6228–6234.

Keller P, Toomre D, Diaz E, White J, Simons K (2001). Multicolour imaging of post-Golgi sorting and trafficking in live cells. Nat Cell Biol 3, 140–149.

Krauss M, Jia JY, Roux A, Beck R, Wieland FT, De Camilli P, Haucke V (2008). Arf1-GTP-induced tubule formation suggests a function of Arf family proteins in curvature acquisition at sites of vesicle budding. J Biol Chem 283, 27717–27723.

Lavieu G, Dunlop MH, Lerich A, Zheng H, Bottanelli F, Rothman JE (2014). The Golgi ribbon structure facilitates anterograde transport of large cargoes. Mol Biol Cell 25, 3028–3036.

Letourneur F, Gaynor EC, Hennecke S, Demolliere C, Duden R, Emr SD, Riezman H, Cosson P (1994). Coatomer is essential for retrieval of dilysine-tagged proteins to the endoplasmic reticulum. Cell 79, 1199–1207.

Lock JG, Stow JL (2005). Rab11 in recycling endosomes regulates the sorting and basolateral transport of E-cadherin. Mol Biol Cell 16, 1744–1755.

Lucy LB ((1974). An iterative technique for the rectification of observed distributions. Astronomical J 79, 745–754.

Lukinavicius G, Reymond L, D'Este E, Masharina A, Gottfert F, TA H, Guther A, Fournier M, Rizzo S, Waldmann H, et al. (2014). Fluorogenic probes for live-cell imaging of the cytoskeleton. Nat Methods 11, 731–733.

Lukinavicius G, Umezawa K, Olivier N, Honigmann A, Yang G, Plass T, Mueller V, Reymond L, Correa IR Jr, Luo ZG, et al. (2013). A near-infrared fluorophore for live-cell super-resolution microscopy of cellular proteins. Nat Chem 5, 132–139.

Martinez-Alonso E, Tomas M, Martinez-Menarguez JA (2013). Golgi tubules: their structure, formation and role in intra-Golgi transport. Histochem Cell Biol 140, 327–339.

McMahon HT, Boucrot E (2011). Molecular mechanism and physiological functions of clathrin-mediated endocytosis. Nat Rev Mol Cell Biol 12, 517–533.

Muller MJ, Klumpp S, Lipowsky R (2010). Bidirectional transport by molecular motors: enhanced processivity and response to external forces. Biophys J 98, 2610–2618.

Ooi CE, Dell'Angelica EC, Bonifacino JS (1998). ADP-ribosylation factor 1 (ARF1) regulates recruitment of the AP-3 adaptor complex to membranes. J Cell Biol 142, 391–402.

Orci L, Stamnes M, Ravazzola M, Amherdt M, Perrelet A, Sollner TH, Rothman JE (1997). Bidirectional transport by distinct populations of COPI-coated vesicles. Cell 90, 335–349.

Ostermann J, Orci L, Tani K, Amherdt M, Ravazzola M, Elazar Z, Rothman JE (1993). Stepwise assembly of functionally active transport vesicles. Cell 75, 1015–1025.

Paczkowski JE, Fromme JC (2014). Structural basis for membrane binding and remodeling by the exomer secretory vesicle cargo adaptor. Dev Cell 30, 610–624.

Palmer DJ, Helms JB, Beckers CJ, Orci L, Rothman JE (1993). Binding of coatomer to Golgi membranes requires ADP-ribosylation factor. J Biol Chem 268, 12083–12089.

Polishchuk EV, Di Pentima A, Luini A, Polishchuk RS (2003). Mechanism of constitutive export from the golgi: bulk flow via the formation, protrusion, and en bloc cleavage of large trans-golgi network tubular domains. Mol Biol Cell 14, 4470–4485.

Popoff V, Adolf F, Brugger B, Wieland F (2011). COPI budding within the Golgi stack. Cold Spring Harb Perspect Biol 3, a005231.

Presley JF, Cole NB, Schroer TA, Hirschberg K, Zaal KJ, Lippincott-Schwartz J (1997). ER-to-Golgi transport visualized in living cells. Nature 389, 81–85.

Presley JF, Smith C, Hirschberg K, Miller C, Cole NB, Zaal KJ, Lippincott-Schwartz J (1998). Golgi membrane dynamics. Mol Biol Cell 9, 1617–1626.

Presley JF, Ward TH, Pfeifer AC, Siggia ED, Phair RD, Lippincott-Schwartz J (2002). Dissection of COPI and Arf1 dynamics in vivo and role in Golgi membrane transport. Nature 417, 187–193.

Puertollano R, Martinez-Menarguez JA, Batista A, Ballesta J, Alonso MA (2001). An intact dilysine-like motif in the carboxyl terminus of MAL is required for normal apical transport of the influenza virus hemagglutinin cargo protein in epithelial Madin-Darby canine kidney cells. Mol Biol Cell 12, 1869–1883.

Puertollano R, van der Wel NN, Greene LE, Eisenberg E, Peters PJ, Bonifacino JS (2003). Morphology and dynamics of clathrin/GGA1-coated carriers budding from the trans-Golgi network. Mol Biol Cell 14, 1545–1557.

Richardson WH ((1972). Bayesian-based iterative method of image restoration. J Opt Soc Am 62, 55–59.

Rivera VM, Wang XR, Wardwell S, Courage NL, Volchuk A, Keenan T, Holt DA, Gilman M, Orci L, Cerasoli F, et al. (2000). Regulation of protein secretion through controlled aggregation in the endoplasmic reticulum. Science 287, 826–830.

Schindelin J, Arganda-Carreras I, Frise E, Kaynig V, Longair M, Pietzsch T, Preibisch S, Rueden C, Saalfeld S, Schmid B, et al. (2012). Fiji: an open-source platform for biological-image analysis. Nat Methods 9, 676–682.

Sciaky N, Presley J, Smith C, Zaal KJ, Cole N, Moreira JE, Terasaki M, Siggia E, Lippincott-Schwartz J (1997). Golgi tubule traffic and the effects of brefeldin A visualized in living cells. J Cell Biol 139, 1137–1155.

Sengupta P, Satpute-Krishnan P, Seo AY, Burnette DT, Patterson GH, Lippincott-Schwartz J (2015). ER trapping reveals Golgi enzymes continually revisit the ER through a recycling pathway that controls Golgi organization. Proc Natl Acad Sci USA 112, E6752–E6761.

Serafini T, Orci L, Amherdt M, Brunner M, Kahn RA, Rothman JE (1991). ADP-ribosylation factor is a subunit of the coat of Golgi-derived COP-coated vesicles: a novel role for a GTP-binding protein. Cell 67, 239–253.

Stamnes MA, Rothman JE (1993). The binding of AP-1 clathrin adaptor particles to Golgi membranes requires ADP-ribosylation factor, a small GTP-binding protein. Cell 73, 999–1005.

Surma MA, Klose C, Simons K (2012). Lipid-dependent protein sorting at the trans-Golgi network. Biochim Biophys Acta 1821, 1059–1067.

Thor F, Gautschi M, Geiger R, Helenius A (2009). Bulk flow revisited: transport of a soluble protein in the secretory pathway. Traffic 10, 1819–1830.

Tokunaga M, Imamoto N, Sakata-Sogawa K (2008). Highly inclined thin illumination enables clear single-molecule imaging in cells. Nat Methods 5, 159–161.

Toomre D, Keller P, White J, Olivo JC, Simons K (1999). Dual-color visualization of trans-Golgi network to plasma membrane traffic along microtubules in living cells. J Cell Sci 112, 21–33.

Traub LM, Ostrom JA, Kornfeld S (1993). Biochemical dissection of Ap-1 recruitment onto Golgi membranes. J Cell Biol 123, 561–573.

Trucco A, Polishchuk RS, Martella O, Di Pentima A, Fusella A, Di Giandomenico D, San Pietro E, Beznoussenko GV, Polishchuk EV, Baldassarre M, et al. (2004). Secretory traffic triggers the formation of tubular continuities across Golgi sub-compartments. Nat Cell Biol 6, 1071–1081.

Waguri S, Dewitte F, Le Borgne R, Rouille Y, Uchiyama Y, Dubremetz JF, Hoflack B (2003). Visualization of TGN to endosome trafficking through fluorescently labeled MPR and AP-1 in living cells. Mol Biol Cell 14, 142–155.

White J, Johannes L, Mallard F, Girod A, Grill S, Reinsch S, Keller P, Tzschaschel B, Echard A, Goud B, et al. (1999). Rab6 coordinates a novel Golgi to ER retrograde transport pathway in live cells. J Cell Biol 147, 743–760.

Yang JS, Valente C, Polishchuk RS, Turacchio G, Layre E, Moody DB, Leslie CC, Gelb MH, Brown WJ, Corda D, et al. (2011). COPI acts in both vesicular and tubular transport. Nat Cell Biol 13, 996–1003.